

Nanohybrid Materials with Tunable Birefringence via Cation Exchange in Polymer Films

Bernette M. Oosterlaken, Yifei Xu, Mark M. J. van Rijt, Marina Pilz da Cunha, Gilles H. Timmermans, Michael G. Debije, Heiner Friedrich, Albertus P. H. J. Schenning,* and Nico A. J. M. Sommerdijk*

In this work, a nanohybrid material based on a freestanding polymeric liquid crystal network capable of postmodification via cation exchange to tune birefringence is proposed. The smectic liquid crystal films can be infiltrated with a variety of cations, thereby changing the refractive indices (n_e and n_o) and the effective birefringence (Δn) of the nanohybrid material, with reversible cation infiltration occurring within minutes. Birefringence could be tuned between values of 0.06 and 0.19, depending on the cation infiltrated into the network. Upon infiltration, a decrease in the smectic layer spacing is found with layer contraction independent of the induced change in birefringence. Potential applications are in the field of specialty optical devices, such as flexible, retunable reflective filters.

devices.^[2] Many nanohybrid materials display extraordinary mechanical and/or optical properties, often arising from alternating organic–inorganic layers.^[3] Of particular interest is the optical property birefringence, which is widely exploited to realize waveplates, optical fibers, and reflective filters.^[4] Production of adjustable optical gratings could also find use in flexible optical beam steering and light intensity modulation.^[5] To extend toward even more advanced optical applications, including displays and smart windows, we are aiming for a nanomaterial with tunable birefringence.^[6]

1. Introduction

Nanohybrid materials have gained significant attention over the past decade.^[1] The interplay between the organic and the inorganic phases generally gives rise to remarkable properties, providing a wide range of potential applications, including biomedical, catalytic, and sensory but also in electrical and optical

Birefringence is known for nanohybrids and polymeric materials and such materials are often used in sophisticated optical applications, such as flexible waveguides.^[7] Although the optical properties of these materials typically can be adjusted during synthesis of the material to meet specific requirements,^[8] it is uncommon that these materials display tunable birefringence after manufacturing.

Liquid crystal networks (LCNs) have been previously used to adsorb silver ions, which could then be reduced to form silver nanoparticles inside the liquid crystalline matrix.^[9] Due to their polymeric nature, these LCNs are excellent frameworks for the selective and reversible adsorption of cations.^[10] Here, we propose a novel postmodification strategy of a LCN to reversibly tune the birefringence through infiltration with cations. In this way, we can set and maintain the birefringence at desired value without the need of a constant external stimulus. It is subsequently possible to reverse the modification and alter the birefringence in the freestanding polymerized film over a range of values.

B. M. Oosterlaken, Dr. Y. Xu, M. M. J. van Rijt, Dr. H. Friedrich, Prof. N. A. J. M. Sommerdijk^[†]
Laboratory of Materials and Interface Chemistry
Center for Multiscale Electron Microscopy
and Institute for Complex Molecular Systems
Eindhoven University of Technology
P.O. Box 513, 5600 MB, Eindhoven, The Netherlands
E-mail: nico.sommerdijk@radboudumc.nl

M. Pilz da Cunha, G. H. Timmermans, Dr. M. G. Debije, Prof. A. P. H. J. Schenning
Stimuli-Responsive Functional Materials and Devices
and Institute for Complex Molecular Systems
Eindhoven University of Technology
P.O. Box 513, 5600 MB, Eindhoven, The Netherlands
E-mail: a.p.h.j.schenning@tue.nl

 The ORCID identification number(s) for the author(s) of this article can be found under <https://doi.org/10.1002/adfm.201907456>.

© 2019 The Authors. Published by WILEY-VCH Verlag GmbH & Co. KGaA, Weinheim. This is an open access article under the terms of the Creative Commons Attribution-NonCommercial License, which permits use, distribution and reproduction in any medium, provided the original work is properly cited and is not used for commercial purposes.

^[†]Present address: Radboud Institute for Molecular Life Sciences, Department of Biochemistry, Geert Grooteplein, 6525 GA, Nijmegen, The Netherlands

DOI: 10.1002/adfm.201907456

2. Results and Discussion

2.1. Preparation of the Liquid Crystal Network and Cation Infiltration

The polymerizable LC mixture used in this work consisted of a hydrogen bonded acid dimer (6OBA, 4-(6-acryloyloxy)hexyloxy) benzoic acid) and a liquid crystalline crosslinker (C6H, 1,4-phenylene bis(4-(6-acryloyloxy)hexyloxy) benzoate). 6OBA and C6H were mixed in a 50/50 w/w ratio to minimize swelling of the material and maintain the network integrity upon base treatment (Figure 1A).^[11] The LC films were formed in rubbed

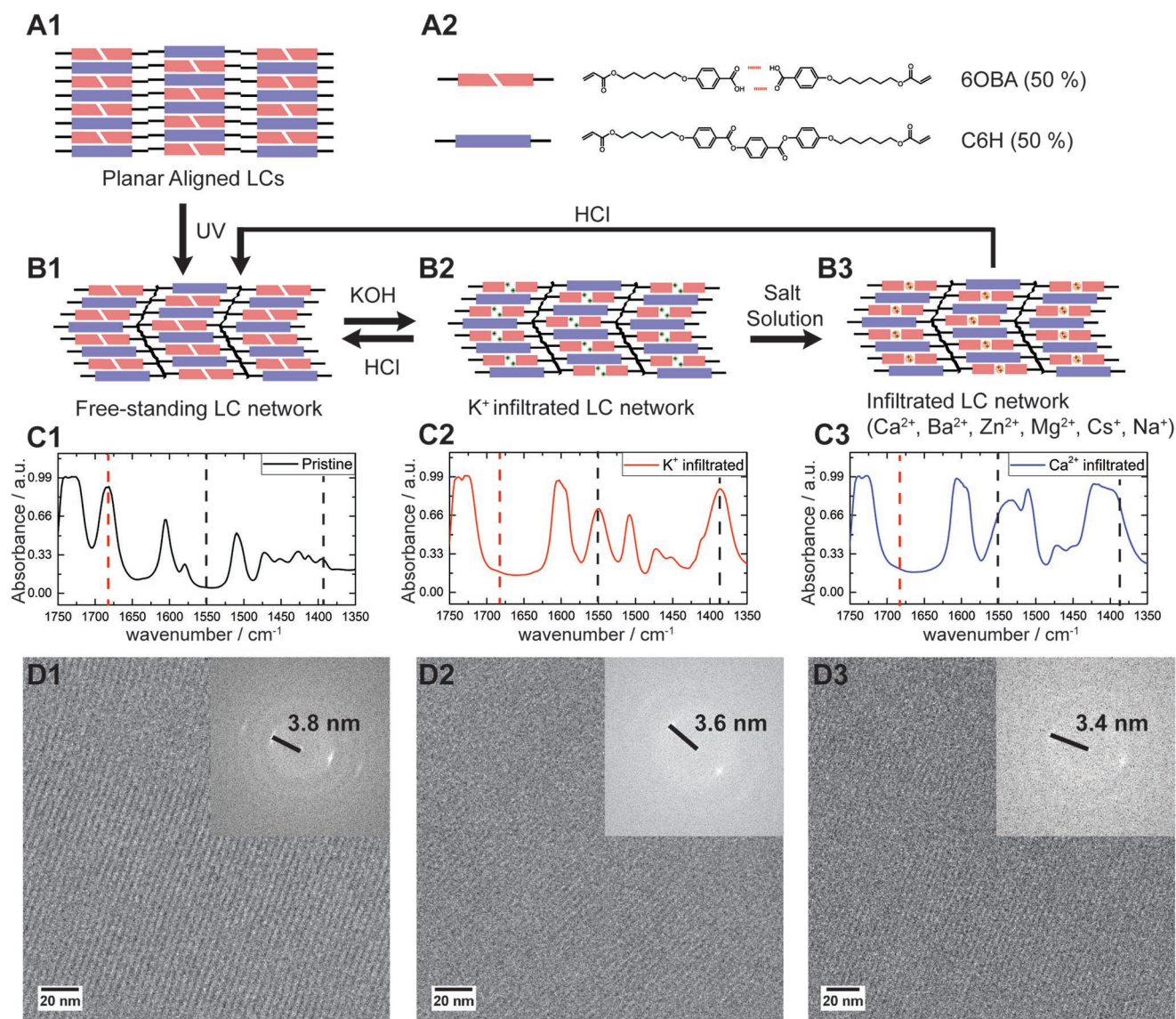


Figure 1. A) Schematic representation of the planar liquid crystals (A1) consisting of a 50/50 w/w mixture of the hydrogen bridged acid dimer 6OBA and the interlayer crosslinker C6H (A2). B) Photopolymerization of the acrylate groups yields a freestanding polymer film (B1). The hydrogen bonds between the 6OBA molecules can be broken via KOH base treatment (B2), after which the network is accessible for the infiltration of other cations (B3). C) The infiltration of cations can be followed using FTIR. Parts of the Fourier transformed transmission infrared spectra (wavenumber 1750–1350 cm^{-1}) are shown for the pristine network (C1), after treatment with KOH (0.5 M, 15 min) (C2) and after exchanging the potassium ions with calcium ions by immersing the film in a 10×10^{-3} M CaCl_2 solution for 24 h (C3). Red dotted lines indicate the disappearance of a peak upon base treatment, while black dotted lines indicate the appearance or shift of a peak. D) TEM images of cross-cut 6OBA/C6H 50/50 w/w LC films for pristine (D1), potassium infiltrated (D2), and calcium infiltrated networks (D3). Scalebar is 20 nm. Insets show the FFT of the image.

polyimide-coated glass cells with 20 μm spacers. The mixture was photopolymerized in the smectic A phase at 95 $^\circ\text{C}$ to fix the layered smectic structure.^[12] Upon photopolymerization, the smectic A structure changes to form a smectic C phase (Figure 1B1),^[13] which could be observed as a chevron-like pattern in polarized optical microscopy images (Figure S1, Supporting Information). The cells were opened, and the films carefully removed from the glass plates using a razor blade to form planarly aligned, freestanding polymer films ≈ 2.5 cm \times 2.5 cm \times 20 μm in size.

The hydrogen bonds between the acid dimers were broken by immersing the freestanding polymer film in a 0.5 M KOH

solution for 15 min, leading to potassium ion infiltration and the formation of a polymer salt (Figure 1B2). The breaking of the hydrogen bonds and the formation of the carboxylate salt were followed using transmission Fourier transform infrared (FTIR) (Figure 1C). After base treatment, the peak indicative of acid dimers at 1680 cm^{-1} in the pristine film^[14] (Figure 1C1) disappeared, while two new peaks appeared at 1550 and 1390 cm^{-1} (Figure 1C2). These latter peaks are associated with the asymmetric and symmetric COO-stretch for carboxylate salts, respectively.^[14]

After this base treatment, which we will from here onwards refer to as K^+ cation infiltration, the polymeric network is

accessible for the infiltration of other cations (Figure 1B3).^[10] By immersing the liquid crystalline network in a 10×10^{-3} M salt solution, the potassium ions were exchanged for Cs^+ , Na^+ , Mg^{2+} , Ca^{2+} , Ba^{2+} , or Zn^{2+} . The cation exchange relies on ionic interactions between the metal ion and the carboxylate. For bivalent ions, binding to two carboxylate groups instead of one, the binding of the metal ion inside the LCN is stronger and therefore favored over monodentate binding. We expect that the potassium ions could be exchanged for other monovalent ions due to a large excess of cations in the exchange solution, competing out the potassium ions over time.

It is known that the IR frequencies for carboxylate salt stretching vibrations are highly dependent on the coordinating metal ion.^[14,15] Indeed, infiltration of cations led to ion-specific peak shifts of the carboxylate peaks in the FTIR spectrum (Figure 1C3 and Figure S2, Supporting Information). In some cases, like for Cs^+ , the shift in IR signal compared to the potassium carboxylate signal is minimal. In those cases, cross-sectional scanning electron microscopy–energy-dispersive X-ray spectroscopy (SEM-EDX) was used to confirm successful cation infiltration (Figure S3, Supporting Information).

Both transmission FTIR and SEM-EDX suggest a homogeneous distribution of cations throughout the film. Moreover, in thermogravimetric analysis (TGA), inorganic fractions of 21.7% and 8.6% were observed, for potassium and calcium ion infiltrated films, respectively (Figure S4, Supporting Information). These values are close to the theoretically calculated inorganic fractions of 22.8% and 12.2%, assuming that all carboxylic acids are converted to carboxylate anions with potassium or calcium counter ions, respectively.^[9,10,16] This suggests full occupation of the carboxylate groups for both monovalent and bivalent cations.

2.2. Tunable Refractive Index and Birefringence upon Cation Infiltration

The Brewster angle (θ_B) was used to calculate the refractive indices of the LCN films before and after cation infiltration. The angle of minimal surface reflection, θ_B , was determined by measuring the reflection intensity of the incoming light beam (400–750 nm) over varying incident angles. The refractive index was calculated via Equation (1)

$$\tan(\theta_B) = n_2/n_1 \quad (1)$$

with n_1 the refractive index of air and n_2 the refractive index of the LC film.

The reflection of light polarized perpendicular to the optic axis is determined by the ordinary refractive index, n_o , and the reflection of light polarized parallel to the optic axis is determined by the extraordinary refractive index, n_e . Once n_e and n_o were determined, the birefringence (Δn) could be calculated via Equation (2)

$$\Delta n = n_e - n_o \quad (2)$$

In Figure 2, the refractive indices and birefringence of the pristine LCN film are shown. Over the wavelength range of

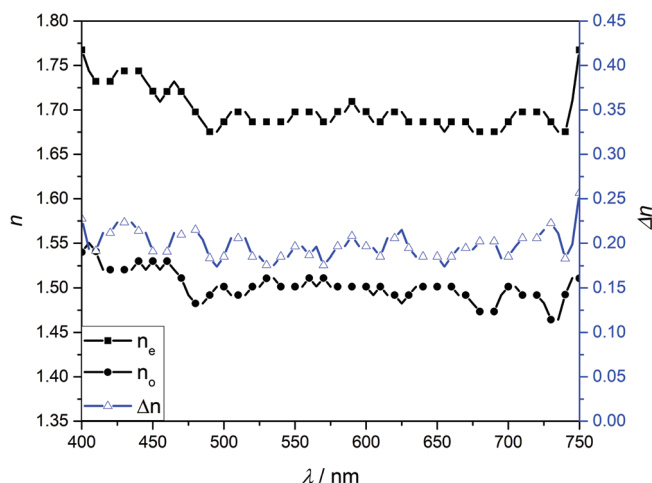


Figure 2. Refractive index (n) and birefringence (Δn) for the pristine 6OBA/C6H (50/50 w/w) liquid crystal film for wavelengths between 400 and 750 nm. The n_e is given in black squares, while n_o is shown in black circles. The birefringence is calculated as $\Delta n = n_e - n_o$ and is plotted as a blue line with open triangles.

400–750 nm, n_e and n_o were relatively constant, ≈ 1.69 and 1.50 , respectively. The deviations around the mean value for the full spectral range are comparable for all LC films (Figure S5, Supporting Information). The averaged values for the refractive indices and birefringence at 590 nm for the pristine and infiltrated LC films are listed in Table 1.

Compared to the pristine LC film, n_e decreased to ≈ 1.58 for all infiltrated LC films. For barium and zinc ion infiltration, n_o increased with respect to the pristine film, while infiltration of potassium or calcium led to a decrease. The changes in both the n_e and the n_o resulted in different birefringences for all infiltrated LC networks. The pristine film has the highest birefringence (0.19 ± 0.03); calcium (0.15 ± 0.03) and potassium (0.12 ± 0.03) infiltrated LC films show a somewhat lower birefringence compared to the pristine film. In contrast, the barium and zinc infiltrated films showed the lowest birefringence with a value of 0.06. Thus, upon cation exchange, the birefringence of the freestanding LC films (Figure S6, Supporting Information) can be tuned between values of 0.06 and 0.19. The birefringence of the polymeric LCN films is comparable to values found for nematic LCs commonly used in LC displays, which have a Δn generally between 0.05 and 0.12.^[17] The birefringence of the LC network nicely falls in the range between quartz ($\Delta n = 0.009$) and rutile (titanium dioxide, $\Delta n = 0.287$), two well-known inorganics that are often employed for their birefringent properties.^[18]

Previous work demonstrated that the cations could be removed from such an infiltrated LC network via acid treatment, thereby restoring the hydrogen bonds between the benzoate monomers,^[16a,19] with high efficiency (over 60%) during multiple adsorption–desorption cycles.^[10] Indeed, when exposing infiltrated LCNs to an acidic solution, the hydrogen bonds are successfully restored between the 6OBA acid dimers, for both K^+ and Ca^{2+} infiltrated films (Figure S7, Supporting Information). Furthermore, after acid treatment, the hydrogen bonds can be broken again by immersing the films in a KOH solution to facilitate infiltration of cations.^[16a]

Table 1. Tunable refractive index and birefringence upon cation infiltration for 6OBA/C6H LC films. The values are given for a wavelength of 590 nm and were calculated by taking the average and standard deviation over wavelengths between 540 and 640 nm (21 data points). The last column gives the refractive index for the corresponding metal oxide at ≈ 530 nm.^[23]

	n_e	n_o	Δn	n of corresponding metal oxide
Pristine	1.69 ± 0.02	1.50 ± 0.02	0.19 ± 0.03	n.a.
K^+	1.59 ± 0.02	1.48 ± 0.02	0.12 ± 0.03	–
Ca^{2+}	1.57 ± 0.02	1.42 ± 0.02	0.15 ± 0.03	1.89
Ba^{2+}	1.59 ± 0.02	1.53 ± 0.05	0.06 ± 0.05	1.99
Zn^{2+}	1.57 ± 0.02	1.51 ± 0.02	0.06 ± 0.03	2.00

Cation infiltration-driven changes in birefringence occur simultaneously with a structural rearrangement in the LC film (see Section 2.3). In situ small angle X-ray scattering (SAXS) experiments (Figure 3) show that K^+ infiltration throughout the bulk of the LC network and structural rearrangement occur rapidly (300 s initiation and 200–300 s rearranging). Thus, cation infiltration allows refractive index tuning of the films under 10 min.

2.3. Structural Rearrangements upon Cation Infiltration

A decrease in the layer spacing in smectic LC networks upon base treatment has been observed previously.^[20] To further investigate the influence of cation infiltration on the network, transmission electron microscopy (TEM) analysis on microtomed cross sections and SAXS measurements were performed (Figures 1 and 4). In contrast to what was previously hypothesized,^[13] the pristine film itself provided sufficient

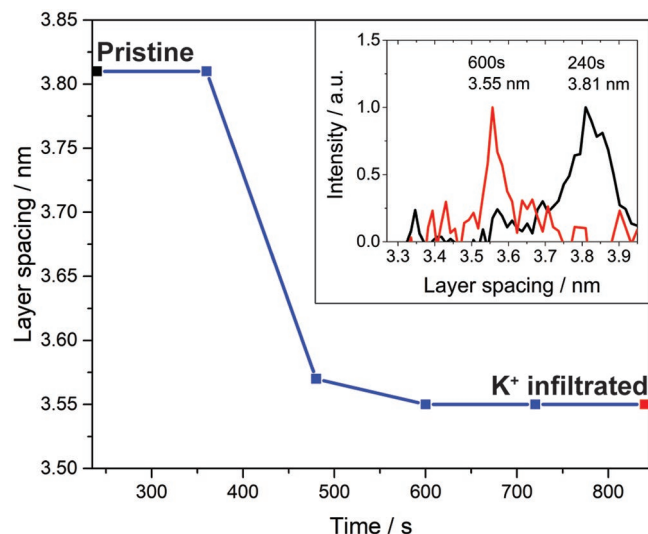


Figure 3. In situ SAXS measurements during K^+ infiltration (0.5 M KOH) show a fast decrease in layer spacing, indicating that the birefringence of the material can be tuned relatively quickly. Inset: 1D plots for the measurements at 240 s (black) and 600 s (red).

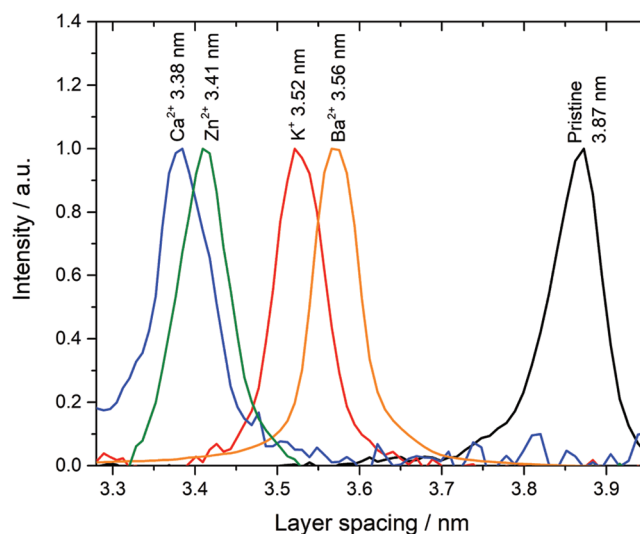


Figure 4. SAXS measurements on the LC films. Normalized 1D plots from SAXS measurements for dried pristine and infiltrated LC films show that the layer spacing decreases upon cation infiltration.

contrast in TEM to visualize the striping pattern associated with the layered smectic LC structure (Figure 1D1). An assignment of the bright and dark stripes to either the benzene rings close to the cation binding site or the alkyl backbone could not be established. When imaging the striping pattern throughout the film, the smectic C orientation proposed in Figure 1B1 is clearly visible (Figure S8 and Movie S1, Supporting Information).^[21]

Analysis of the TEM images by fast Fourier transform (FFT) showed that sharp peaks are present which indicates highly directional layers with uniform layer spacing both before and after cation infiltration. The layer periodicity was accurately measured from the position of the peaks in the FFTs, with a layer spacing of 3.8 nm found in pristine LCN. For potassium and calcium infiltrated films (Figure 1D2,D3), the layer spacing decreased to 3.6 and 3.4 nm, respectively. Using SAXS, the layer spacing and orientation throughout the bulk of the liquid crystalline films were also determined (Figure 4 and Figure S9, Supporting Information) and matched well to the layer spacings determined with TEM. All tested cation exchanges led to decreases in the smectic layer spacing, while maintaining the smectic C structure (Figure S10, Supporting Information).

Surprisingly, the decreases in layer spacings upon cation infiltration appear unrelated to the size or charge of the ions. Zinc, for example, has the smallest ionic radius (0.68 Å)^[22] but does not result in the smallest layer spacing. One must consider that the size of the ions is not fixed in aqueous environments, as the ions are surrounded by coordinating water molecules. This hydration shell depends on the size, charge, and chemical environment of the ion, and the carboxylic acid binding to metal ions is influenced by the hydration layers around the cation.^[23] Therefore, it is difficult to predict the ionic radii or the binding geometry of the infiltrated cations in general, nor their effect on the smectic layer spacing.^[24] Nevertheless, it can be argued that for Ca^{2+} ions, which are known to favor a bidentate binding to the carboxylate group,

a planar carboxylate-calcium complex may be formed,^[16a,25] which would explain the pronounced decrease in layer spacing to 3.38 nm (Figure 4).

2.4. Linking LC Morphology/Structure to Birefringence

The changes in the effective refractive index and birefringence of the films could be caused by several structural/morphological changes: i) the variation of smectic layer thicknesses, ii) the tilt angles of the LCs in the smectic layers, iii) the formation of inorganic crystals within the LC pores, or iv) are simply related to the nature of the infiltrated metal itself. Each possibility will be discussed in detail next.

When comparing the variations in layer spacing with changes in birefringence, it becomes clear that they are not directly related. For example, the pristine LC film has the largest layer spacing (3.8 nm) and the highest birefringence (0.19), while the barium infiltrated film has the second largest layer spacing (3.6 nm) but the lowest birefringence (0.05). The calcium infiltrated film, on the other hand, has the smallest layer spacing (3.4 nm) but the second highest birefringence (0.15). Similarly, there appears to be no relation between the changes in refractive indices and the decreases in layer spacing upon cation infiltration. Thus, variations in birefringence and refractive indices seen in the infiltrated films are not the result of the decreased layer spacing in the LC network.

The decrease in layer spacing is potentially associated with a changing tilt angle of the LC monomers. The molecular order in the LC-based nanohybrid materials was monitored using wide angle X-ray scattering (WAXS): upon breaking the hydrogen bonds with potassium hydroxide, we observe that the WAXS signal becomes slightly more isotropic, suggesting that a range of molecular tilt angles may be present within the infiltrated films (Figure S11, Supporting Information). However, the WAXS signals of the films showed near-identical shapes for all the different infiltrated cations, indicating the different nanohybrids all had a similar molecular order, likely due to the inflexibility of the highly crosslinked network (50% crosslinker in the network). Thus, it is concluded that the birefringence is not related to changes in the molecular ordering of the LC monomers.

To investigate whether the changes in refractive index and birefringence are due to crystal formation *inside* the LC films, WAXS measurements were performed (Figure S12, Supporting Information). No crystalline signals were found in the infiltrated polymer films, indicating that no crystals were formed inside the LC film during cation infiltration. This shows that the changes in refractive index and birefringence are not due to the presence of crystalline material within the LC films.

The discussion above leads us to conclude that the changes of optical properties in these ion-infiltrated LC films are primarily dependent on the nature of the cation. To support this conclusion, we performed a systematic study in which we compared the birefringence of the LC films with the refractive indices of the corresponding metallic oxides (Table 1).^[26] As can be seen, the birefringence of the infiltrated films roughly follows the refractive index with the higher birefringence values corresponding to cations having a low refractive index oxide. Assuming that the contribution of the oxygen atoms in the

face-centered cubic crystal lattices is the same for each metallic oxide, it has to be the optical nature of the cation that is responsible for the differences in refractive index between various metal oxides, but also for the changes in birefringence between the different infiltrated LCNs. Thus, the optical nature of the cation is mainly responsible for tuning of the birefringence in ion-infiltrated LC networks.

3. Conclusion

We have shown a novel approach of tuning the birefringence of a polymeric freestanding 6OBA/C6H (50/50 w/w) smectic LC network via infiltration of cations. Infiltrated potassium ions into the LC system may be quickly exchanged for other cations (5 min initiation and 3–5 min for rearrangements), thereby creating a nanohybrid material. This allowed specific tuning of the refractive indices (n_o and n_e), and thus the effective birefringence (Δn) of the material.

When cations are infiltrated into the LC network, the layer spacing of the smectic LC network decreases. However, the changes in refractive index are neither related to the layer spacing nor to crystal formation inside the LC network, indicating that the changes in refractive index and birefringence are only the result of the nature of the cation.

Cation exchange in the smectic LC network provides a relatively inexpensive, reversible, and easy postmodification to specifically tune the birefringence of the freestanding material to a desired value. Moreover, we can maintain the birefringence at a specific value without the constant use of an external stimulus, suggesting future application in the fields of specialty optics such as smart windows and reflective filters.

4. Experimental Section

Materials: The hydrogen bridged 6OBA and the interlayer liquid crystalline crosslinker, C6H were both custom made by Synthron Chemicals, Germany. Initiator 1-hydroxycyclohexylphenylketone (Igracure 184) was supplied by Ciba Specialty Chemicals. Inhibitor p-methoxyphenol, CaCl₂, MgCl₂, BaCl₂, NaCl, Cs₂CO₃, and Zn(CH₃COO)₂ were purchased from Sigma Aldrich. Solvents were analytical grade and obtained from Biosolve. All reagents were used as received, without further purification.

Preparation of the Liquid Crystalline Network: A LC mixture was prepared by mixing the hydrogen bridged 6OBA with the liquid crystalline crosslinker C6H in a 50/50 w/w ratio. 0.5 wt% of photoinitiator Igracure 184 was added for photopolymerization. 0.1 wt% of thermal inhibitor was added to the mixture. The compounds were dissolved in dichloromethane, which was evaporated after mixing.

Glass plates were coated with a rubbed polyimide alignment layer (OPTMER AL 1051) to obtain planar alignment of the LCs. Films with a thickness of 20 μm were made by processing the mixture in the melt at 120 °C via capillary suction between two polyimide-coated glass plates affixed together with glue containing spacers. After filling the cell, the films were cooled rapidly to 105 °C. The cooling process was continued with 1 °C min⁻¹ to 95 °C. The films were photopolymerized at 95 °C for 10 min with UV irradiation using an EXFO OmniCure S2000 spot UV-curing lamp. The LC films were carefully removed from the substrate using a razor blade.

Cation Infiltration: The hydrogen bonds between the 6OBA monomers were broken by immersing the liquid crystalline freestanding films in a 0.5 M KOH solution for 15 min. The K⁺ ions were exchanged for other ions

(Ca²⁺, Mg²⁺, Ba²⁺, Cs⁺, and Zn²⁺) by immersing the film in 10×10^{-3} M salt solutions (CaCl₂, MgCl₂, BaCl₂, NaCl, Cs₂CO₃, ZnNO₃) for 24 h, to ensure that all K⁺ ions were exchanged. After infiltration, the films were dried on filter paper. The infiltration of ions was checked using FTIR in transmission mode on a Varian 670 IR spectrometer over a range of 4000–650 cm⁻¹ with a spectral resolution of 4 cm⁻¹ and 100 scans per spectrum.

Supporting Information

Supporting Information is available from the Wiley Online Library or from the author.

Acknowledgements

The work of B.M.O., Y.X., and M.M.J.v.R. was supported by a TopPunt grant of the Netherlands Organisation for Scientific Research (NWO) to N.A.J.M.S. and A.P.J.H.S. M.P.d.C. was funded by Technology Foundation STW and the Impuls 2 program of the TU/e. The authors thank Prof. Dick Broer and Ing. Tom Bus for their help with the birefringence measurements and helpful discussions. The authors thank Dr. Daniel Hermida Merino from Beamline 26B at the ESRF Grenoble, France, for his help with the SAXS and WAXS measurements.

Conflict of Interest

The authors declare no conflict of interest.

Keywords

birefringence, cation infiltration, liquid crystals, nanohybrid materials, tunable optical properties

Received: September 9, 2019

Revised: October 28, 2019

Published online: December 9, 2019

- [1] L.-H. Liu, R. Métivier, S. Wang, H. Wang, *J. Nanomater.* **2012**, 2012, 1.
- [2] a) C. He, D. Liu, W. Lin, *Chem. Rev.* **2015**, 115, 11079; b) L. Nicole, L. Rozes, C. Sanchez, *Adv. Mater.* **2010**, 22, 3208; c) C. Sanchez, B. Lebeau, F. Chaput, J. P. Boilot, *Adv. Mater.* **2003**, 15, 1969; d) K. Gregorczyk, M. Knez, *Prog. Mater. Sci.* **2016**, 75, 1; e) A. G. Thawari, C. P. Rao, *ACS Appl. Mater. Interfaces* **2016**, 8, 10392.
- [3] F. Nudelman, H. H. Chen, H. A. Goldberg, S. Weiner, L. Addadi, *Faraday Discuss.* **2007**, 136, 9.
- [4] a) T. R. Wolinski, S. Ertman, P. Lesiak, A. W. domanski, A. Czaplá, R. Dabrowski, E. Nowinowski-Kruszelnicki, J. Wojcik, *Opto-Electron. Rev.* **2006**, 14, 329; b) T. R. Wolinski, A. Czaplá, S. Ertman, M. Tefelska, A. W. Domanski, E. Nowinowski-Kruszelnicki, R. Dabrowski, *Opt. Quantum Electron.* **2007**, 39, 1021; c) H. Yang, H. Jussila, A. Autere, H.-P. Komsa, G. Ye, X. Chen, T. Hasan, Z. Sun, *ACS Photonics* **2017**, 4, 3023.
- [5] a) M. L. Jepsen, H. J. Gerritsen, *High-Efficiency Liquid-Crystal-Filled Diffraction Gratings*, SPIE, Bellingham, WA **1997**; b) G. Rodriguez, A. J. Taylor, *Opt. Lett.* **1996**, 21, 1046.
- [6] a) P. Kirsch, M. Bremer, *Angew. Chem.* **2000**, 39, 4216; b) Q. Liu, A. W. Frazier, X. Zhao, J. A. De La Cruz, A. J. Hess, R. Yang, I. I. Smalyukh, *Nano Energy* **2018**, 48, 266.
- [7] a) B. Lebeau, P. Innocenzi, *Chem. Soc. Rev.* **2011**, 40, 886; b) M.-C. Oh, W.-S. Chu, J.-S. Shin, J.-W. Kim, K.-J. Kim, J.-K. Seo, H.-K. Lee, Y.-O. Noh, H.-J. Lee, *Opt. Commun.* **2016**, 362, 3; c) H. Ma, A. K. Y. Jen, L. R. Dalton, *Adv. Mater.* **2002**, 14, 1339.
- [8] M. D. Barnes, C. Y. Kung, N. Lermer, K. Fukui, B. G. Sumpter, D. W. Noid, J. U. Otaigbe, *Opt. Lett.* **1999**, 24, 121.
- [9] D. Dasgupta, I. K. Shishmanova, A. Ruiz-Carretero, K. Lu, M. Verhoeven, H. P. C. van Kuringen, G. Portale, P. Leclere, C. W. M. Bastiaansen, D. J. Broer, A. P. H. J. Schenning, *J. Am. Chem. Soc.* **2013**, 135, 10922.
- [10] H. P. C. van Kuringen, G. M. Eikelboom, I. K. Shishmanova, D. J. Broer, A. P. H. J. Schenning, *Adv. Funct. Mater.* **2014**, 24, 5045.
- [11] a) I. K. Shishmanova, C. W. M. Bastiaansen, A. P. H. J. Schenning, D. J. Broer, *Chem. Commun.* **2012**, 48, 4555; b) T. Liang, H. P. C. van Kuringen, D. J. Mulder, S. Tan, Y. Wu, Z. Borneman, K. Nijmeijer, A. Schenning, *ACS Appl. Mater. Interfaces* **2017**, 9, 35218.
- [12] E. Peeters, J. Lub, J. A. M. Steenbakkers, D. J. Broer, *Adv. Mater.* **2006**, 18, 2412.
- [13] C. L. Gonzalez, C. W. M. Bastiaansen, J. Lub, J. Loos, K. Lu, H. J. Wondergem, D. J. Broer, *Adv. Mater.* **2008**, 20, 1246.
- [14] G. Socrates, *Infrared and Raman Characteristic Group Frequencies*, Wiley, Chichester, UK **2001**.
- [15] N. B. Colthup, L. H. Daly, S. E. Wiberley, *Introduction to Infrared and Raman Spectroscopy*, Academic, Boston, MA **1990**.
- [16] a) M. Moirangthem, R. Arts, M. Merx, A. P. H. J. Schenning, *Adv. Funct. Mater.* **2016**, 26, 1154; b) M. Ghiasi, A. Malekzadeh, *Cryst. Res. Technol.* **2012**, 47, 471.
- [17] a) R. Dabrowski, P. Kula, J. Herman, *Crystals* **2013**, 3, 443; b) Y. Garbovskiy, V. Zagorodnii, P. Krivosik, J. Lovejoy, R. E. Camley, Z. Celinski, A. Glushchenko, J. Dziaduszek, R. Dąbrowski, *J. Appl. Phys.* **2012**, 111, 054504.
- [18] a) G. Elert, *The Physics Hypertextbook*, <https://physics.info/refraction/> (accessed: December 2018); b) E. Collet, *Polarized Light in Fiber Optics* The PolaWave Group, Lincroft, NJ **2003**.
- [19] M. Moirangthem, A. P. H. J. Schenning, *ACS Appl. Mater. Interfaces* **2018**, 10, 4168.
- [20] H. P. C. van Kuringen, *Ph.D. Thesis*, Eindhoven University of Technology, **2016**.
- [21] K. Gnanasekaran, R. C. Q. Snel, G. de With, H. Friedrich, *Ultramicroscopy* **2016**, 160, 130.
- [22] R. D. Shannon, *Acta Crystallogr.*, **A 1976**, 32, 751.
- [23] a) T. Dudev, C. Lim, *J. Am. Chem. Soc.* **2013**, 135, 17200; b) C. Wagner, M. Blank, M. Oetken, *CHEMKON* **2018**, 25, 57; c) G. Schwaab, F. Sebastiani, M. Havenith, *Angew. Chem., Int. Ed.* **2019**, 58, 3000.
- [24] B. Tansel, J. Sager, T. Rector, J. Garland, R. F. Strayer, L. F. Levine, M. Roberts, M. Hummerick, J. Bauer, *Sep. Purif. Technol.* **2006**, 51, 40.
- [25] T. Dudev, C. Lim, *J. Phys. Chem. B* **2004**, 108, 4546.
- [26] a) C. J. Liu, E. F. Sieckmann, *J. Appl. Phys.* **1966**, 37, 2450; b) C. J. Anderson, E. B. Hensley, *J. Appl. Phys.* **1975**, 46, 443; c) W. L. Bond, *J. Appl. Phys.* **1965**, 36, 1674.